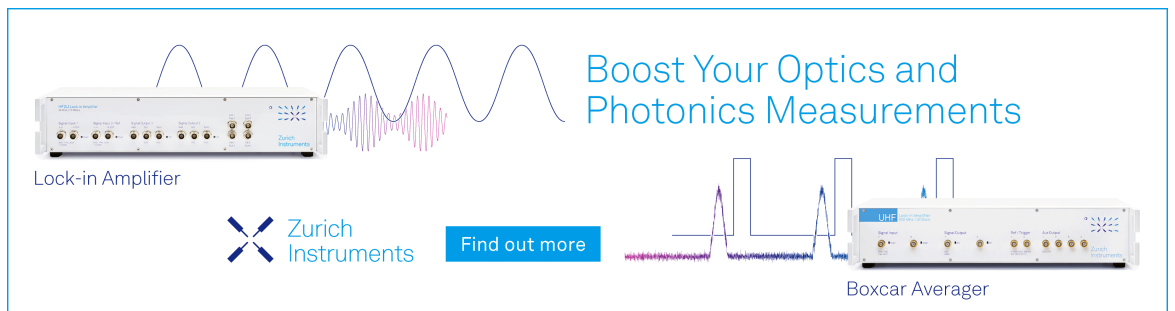# Effects of electrostatic coupling and surface polarization on polyelectrolyte brush structure ⊘

Igor M. Telles ⓘ ; Muhammad Arfan ⓘ ; Alexandre P. dos Santos ✉ ⓘ

Check for updates

View Online   Export Citation

AIP Publishing

Effects of electrostatic coupling and surface polarization on polyelectrolyte brush structure

Igor M. Telles,[a] [ID] Muhammad Arfan,[b] [ID] and Alexandre P. dos Santos[c] [ID]

AFFILIATIONS

Instituto de Física, Universidade Federal do Rio Grande do Sul, Caixa Postal 15051, CEP 91501-970 Porto Alegre, RS, Brazil

[a] Electronic mail: igor.morais@ufrgs.br
[b] Electronic mail: muhammad.arfan@ufrgs.br
[c] Author to whom correspondence should be addressed: alexandre.pereira@ufrgs.br

ABSTRACT

In this work, we perform molecular dynamics simulations to study a spherical polyelectrolyte brush. We explore the effects of surface polarization and electrostatic coupling on brush size and distribution of counterions. The method of image charges is considered to take into account surface polarization, considering a metallic, an unpolarizable, and a dielectric nano-core. It is observed that, for all cases, a moderate shrinking–swelling effect appears with an increase in the electrostatic coupling parameter. This effect occurs under high Manning ratios. The curves relating the average size of polyelectrolyte brush as a function of coupling show a minimum. The results show that the grafting density of polyelectrolytes on the nano-core surface plays an important role in the polarization effect. We consider a modified Poisson–Boltzmann theory to describe the counterion profiles around the brush in the case of unpolarizable nano-cores and weak electrostatic coupling.

Published under an exclusive license by AIP Publishing. https://doi.org/10.1063/5.0147056

I. INTRODUCTION

Polyelectrolyte brushes (PEBs) are nano- or micro-structures formed by organic charged polymer chains grafted to inorganic surfaces in diverse geometries.[1–5] In recent years, the study of PEBs has acquired considerable interest due to their importance in several applications, such as biological lubrication,[6] anti-fouling,[7] anti-icing,[8] and adhesives.[9] The PEBs have shown their importance in ionic current rectification[10–12]—an important phenomenon of the modern area of iontronics, along with applications in microfluidic devices.[13,14] In particular, spherical PEBs have been synthesized to be considered for optical applications,[15] nanoreactions,[16] drug delivery,[17] and colloidal stabilization.[18] The development of new methods in nanotechnology opens up the possibility for a wide range of new applications.[19–22]

The shrinking and swelling properties of PEBs, in multiple geometries, affect most of the applications mentioned above.[23–29] These depend on various aspects, such as screening salt concentration,[30] applied external field,[31] pH,[32,33] electrostatic correlations,[34] chain grafting density,[35] and ionic specificity.[36] They can control the fluid flow inside brush pores[37] and the friction of cationic and anionic brushes.[38] The distribution of ions around the PEB has

a crucial influence on its size as, for weak electrostatic correlations, the brush layer is swollen by the osmotic pressure of the counterions, while at intermediate salt concentrations, they shrink the brush structure due to partial screening of the electrostatic interactions.[39]

In general, the dielectric constant of the brush nano-core is considered to be the same as that of the exterior, which means that polarization effects are neglected. However, it is known that, for example, phase diagrams in membrane stacks,[40] counterions distribution around colloids,[41,42] colloidal self-assembly,[43] interaction between ionic clusters,[44] and electro-osmotic flow[45,46] depend on surface polarization. Using molecular dynamics simulations in the case of a low dielectric constant brush nano-core, it was shown that polarization effects are marginal, even for trivalent counterions at room temperature.[47] In other rare publications, the brush surface polarizability was explored in a planar geometry, showing the importance of surface polarization to ion mobility through the brushes[48] and to the brush structure.[49] In the mentioned work,[49] the authors studied the effects of several parameters on the planar PEB structure, such as the Bjerrum length and grafting density. One of the main findings is the intra- and inter-chain condensation of trivalent counterions for conducting surfaces. The results show the

importance of electrostatic correlations and surface polarization in the equilibrium properties of PEBs.

In this paper, we show the effects of surface polarization and electrostatic correlations on the distribution of counterions around a metallic, unpolarizable, and dielectric spherical polyelectrolyte brush nano-core. For all cases, a moderate shrinking–swelling effect is observed when increasing the electrostatic coupling parameter. For a higher grafting density, 0.069 chains per nm^2, the results obtained for unpolarizable and metallic nano-cores are very similar, while for a lower density, 0.0027 chains per nm^2, the brush nano-core polarization highly influences the polyelectrolyte brush. It has to do with the more available free space in polarizable surfaces for ion–surface interaction, in the case of a lower grafting density. In this case, the conductive surface adsorbs plenty of counterions due to surface polarization, leaving few ions to neutralize the charged chains. The charged chains are then not neutralized, carrying an excess of charge, which allows them to strongly stick to the nano-core surface. For the other cases, the counterions adsorb to the oppositely charged polymer chains instead of the nano-core surface, neutralizing almost all of them and forming quasi-globular or stretched structures. For dielectric nano-cores in the strong coupling limit, a tree-like structure for polyelectrolytes is observed, related to the image charge repulsion from the surface. In the weak coupling regime and unpolarizable nano-core, we compare the simulation results with a modified Poisson–Boltzmann (mPB) theory. The computational simulations are performed using Langevin molecular dynamics.[50,51] The method of image charges is considered for electrostatic interactions,[41,47,52] while a truncated Lennard-Jones potential avoids particles overlap. The adjacent monomers in the brush are connected via a harmonic potential. In Sec. II, we show the model and details considered, followed by the mean-field theory. After that, results and conclusions are presented.

II. MODEL AND SIMULATION DETAILS

The molecular dynamics simulations are performed inside a spherical cell of radius R with a uniform dielectric constant ε_w; see Fig. 1(a). The centered nanoparticle has a radius a and a uniform dielectric constant ε_c. The dielectric contrast is defined as $\gamma = (\varepsilon_w - \varepsilon_c)/(\varepsilon_w + \varepsilon_c)$. The first monomer of $N_p = 14$ polyelectrolyte chains is uniformly distributed and attached to the nano-core surface at a distance $a + r_c$ from the center, where r_c is the effective particle radius. Each chain is made of N_m monomers with a centered charge $+\alpha q$, where α is the ionic valence and q is the proton charge. Inside the cell but outside the nanoparticle, there are $N_c = N_p N_m$ counterions of charge $-\alpha q$. All particles have an effective ionic radius $r_c = 2$ Å. The natural length scale in the present simulation is the particle diameter, $d = 2r_c$. In this way, we can define the coupling parameter as $\Xi = \alpha^2 l_B/d$, where $l_B = q^2/\varepsilon_w k_B T$ is the Bjerrum length. The coupling parameter is explored from 1 to 100. For conducting nano-cores, $\gamma = -1$, low coupling parameters can represent monovalent ions at room temperature in water, while high values can represent the same but in oil, as it has a low dielectric constant. In the case of a low dielectric constant solution, the polarizable insulating scenario is meaningless because a silica nano-core, for example, also has a low dielectric constant. The dielectric case, $\gamma = 0.95$, can
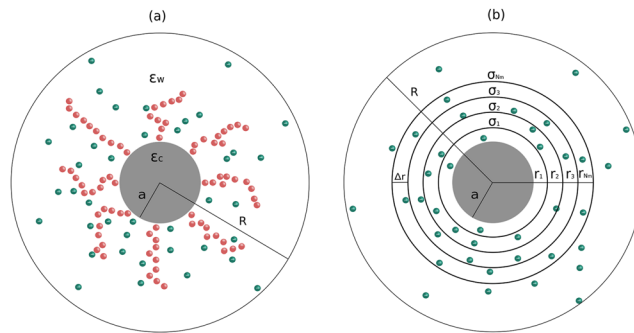

FIG. 1. (a) Schematic illustration of the studied system. A nanoparticle of radius a and dielectric constant ε_c is centered at the spherical cell of radius R. The polyelectrolyte chains are grafted to the nanoparticle surface, and the counterions are distributed over the aqueous medium of dielectric constant ε_w. (b) Model for the mean-field theory. The chain monomers are uniformly distributed over radial layers.

model a silica nano-core in water. In this case, high coupling parameters can be achieved, for example, with a combination of low temperatures and high ionic valences.

The harmonic interaction potential between adjacent monomers in chains is given by[53]

$$U_{adj} = \frac{\Gamma_b}{2}\left(r_i^{adj} - r_0\right)^2, \tag{1}$$

where r_i^{adj} is the distance between monomer i and the next adjacent monomer, $r_0 = (3/2)d$, and Γ_b is the bond potential constant. We set $\Gamma_b = 2k_B T/d^2$. The Manning ratio[54] is defined as $\xi = l_B/r_0$, and it can be rewritten as $\xi = 2\Xi/3\alpha^2$. This means that, for fixed valencies, the Manning ratio and the coupling parameter are proportional. For monovalent ions, the Manning ratios are ~0.67, 33, and 67 for couplings $\Xi = 1$, $\Xi = 50$, and $\Xi = 100$, respectively. Most cases in this work consider ratios above the corresponding Manning counterion condensation phenomenon. All particles interact through a truncated Lennard-Jones potential,

$$U_{LJ} = \Theta(r_{cut} - r_{ij})\left(4\Gamma_{lj}\left[\left(\frac{d}{r_{ij}}\right)^{12} - \left(\frac{d}{r_{ij}}\right)^6\right] + \Gamma_{lj}\right), \tag{2}$$

where $\Gamma_{lj} = 2k_B T$, r_{ij} is the distance between particles i and j, $\Theta(x)$ is the Heaviside step function, and $r_{cut} = 2^{1/6}d$.

In the case of a conducting spherical nanoparticle, $\varepsilon_c \to \infty$, the interaction potential between particles i and j at positions $\mathbf{r}_i$ and $\mathbf{r}_j$ is given using the image charges method,[52,55]

$$\beta U_e^c = \alpha^2 l_B s_i s_j \frac{1}{|\mathbf{r}_i - \mathbf{r}_j|} + \frac{\alpha^2 l_B a s_i s_j}{r_j}\left[\frac{1}{|\mathbf{r}_i|} - \frac{1}{|\mathbf{r}_i - \frac{a^2}{r_j^2}\mathbf{r}_j|}\right], \tag{3}$$

where $s_i = +1$ is for monomers and $s_i = -1$ for counterions. The distance r_j is given by $r_j = |\mathbf{r}_j|$.

When the nanoparticle has a dielectric constant much lower than the outside medium, $\varepsilon_c \ll \varepsilon_w$, the electrostatic interaction is also given by the method of image charges,[41,47]

$$\beta U_e^d = \alpha^2 l_B s_i s_j \frac{1}{|\mathbf{r}_i - \mathbf{r}_j|} + \alpha^2 l_B s_i s_j \left[\frac{\gamma a}{r_i |\mathbf{r}_j - \frac{a^2}{r_i^2}\mathbf{r}_i|} \right.$$
$$\left. + \frac{\gamma}{a} \ln \left(\frac{r_i r_j - \mathbf{r}_i \cdot \mathbf{r}_j}{a^2 - \mathbf{r}_i \cdot \mathbf{r}_j + \sqrt{a^4 - 2a^2(\mathbf{r}_i \cdot \mathbf{r}_j) + r_i r_j}} \right) \right]. \quad (4)$$

It is important to mention that the particles also interact with their self-image charges.

The motion of particles is governed by the well-known Langevin dynamics. The integration is performed using the velocity-Verlet algorithm, considering the time step $dt = 0.005\,d(m\beta)^{1/2}$, where m is the mass of all particles. It is important to notice that since the first monomer of each polyelectrolyte chain is grafted to the nanoparticle surface, its velocity is zero along the simulation. The statistical analysis is performed over the 5×10^4 samples obtained each ten time steps after the equilibrium, which takes $\sim 1 \times 10^5$ time steps. The bounce-back technique is used to prevent particles from getting into the nanoparticle and also to keep it inside the spherical cell. We wrote all codes used to perform simulations and to analyze the data.

III. MODIFIED POISSON–BOLTZMANN THEORY

In order to study tethered charged chains, some works considered field theory,[56,57] scaling,[5,58] density functional theory,[59] and the so-called molecular theory.[60] We use a simple mPB equation to study the ionic concentration around the brush in the case of an unpolarizable nanoparticle.[47] It is known that the PB equation works well in the limit of weak electrostatic correlations.[61] The present model is constructed as if all the monomers are aligned with the nanoparticle center and uniformly located at radial layers; see Fig. 1(b). The mPB equation is[47]

$$\nabla^2 \phi(r) = -\frac{4\pi}{\varepsilon_w} \left[\sum_{k=1}^{N_m} \sigma_k \delta(r - r_k) - \alpha q \rho_-(r) \right], \quad (5)$$

where the charge density of the corresponding layers of monomers are

$$\sigma_k = \frac{\alpha q N_p}{4\pi r_k^2}, \quad \text{where } r_k = r_{k-1} + \Delta r(N_m). \quad (6)$$

The first layer is at contact, $r_1 = a + r_c$, while ρ_- is the concentration of counterions inside the cell. The distance between layers, Δr, was previously defined as a constant,[47] not resulting in good agreement between theory and simulations for longer chains.[47] In order to improve the validity of this theory, let us consider that the chain's length is proportional to the square root of the number of monomers, $\propto \sqrt{N_m}$, considering the 1D random walk approximation. This means that the separation between layers is $\propto \sqrt{N_m}/N_m$,

$$\Delta r(N_m) = b \frac{r_c}{\sqrt{N_m}}, \quad (7)$$

where $b = 11$. The constant was obtained from fitting the simulation data solely for the first case discussed in Sec. IV. The mPB equation can be solved by the Picard iterative process. A more complex definition of Δr will guarantee that it works for polarizable cases and in the presence of salt. This is going to be developed in future work.

IV. RESULTS AND DISCUSSION

Here, we show the results of two distinct cases, a small nano-core PEB with a radius $a = 40$ Å and charged chains with $N_m = 30$ monomers and a big nano-core PEB with a radius $a = 200$ Å and chains with $N_m = 60$ monomers. Both cases represent a chain grafting density of 0.069 chains per nm^2 and 0.0027 chains per nm^2, respectively. For both systems, we fix the number of charged chains at $N_p = 14$. We separately study each case in the following.

A. Small nano-core

Let us consider the small polarizable nanoparticle with $N_p = 14$ attached polyelectrolytes. The nano-core radius is $a = 40$ Å, while the confining cell radius is $R = 250$ Å. The brush grafting density is 0.069 chains per nm^2. The number of monomers in each chain is $N_m = 30$. In Fig. 2, the ionic and monomer concentration profiles are shown for three polarizable cases, $\gamma = -1$, 0, and 0.95, representing metallic, unpolarizable, and dielectric cores, respectively. In addition, we consider three coupling parameters, $\Xi = 1$, 50, and 100. In the previous work, we have considered just the dielectric nano-core and low coupling parameters.[47] For an unpolarizable nano-core and a weak coupling parameter, we solve the mPB equation, Eq. (5). It is natural that the increment Δr in the mPB equation depends on the number of monomers in the chain. We obtain the constant $b = 11$ in Eq. (7), from the best fit of the simulation result; see the black line in Fig. 2. The theory is going to be generalized in future work, considering added salt concentrations and the nano-core polarization.

For all cases, the ionic adsorption is strong for higher coupling parameters. In charged colloids, the increase in the coupling parameter leads to stronger ionic adsorption. This is not the case for polyelectrolyte brushes. For coupling $\Xi = 100$, we observe less adsorption than for $\Xi = 50$, in all studied cases. This is related to the shrinking–swelling effect discussed in the following. The metallic and unpolarizable cases are very similar, while the dielectric case shows a peculiar behavior of counterions and monomers due to repulsion from the dielectric surface. This is also observed in the PEB size, R_B, defined as the average distance between the nano-core center and the most distant monomer in the chains,

$$R_B = \left\langle \frac{1}{N_p} \sum_{i=1}^{N_p} r_i^{(m)} \right\rangle, \quad (8)$$

where $r_i^{(m)}$ is the distance between the center of the PEB nano-core and the most distant monomer in chain i. In Fig. 3, we show the size R_B as a function of the coupling parameter for three polarization cases. The size of PEBs decreases with an increase in the electrostatic coupling parameter. This is expected as the adsorption of counterions to charged monomers in chains becomes more and more important. It is well known that multivalent counterions in
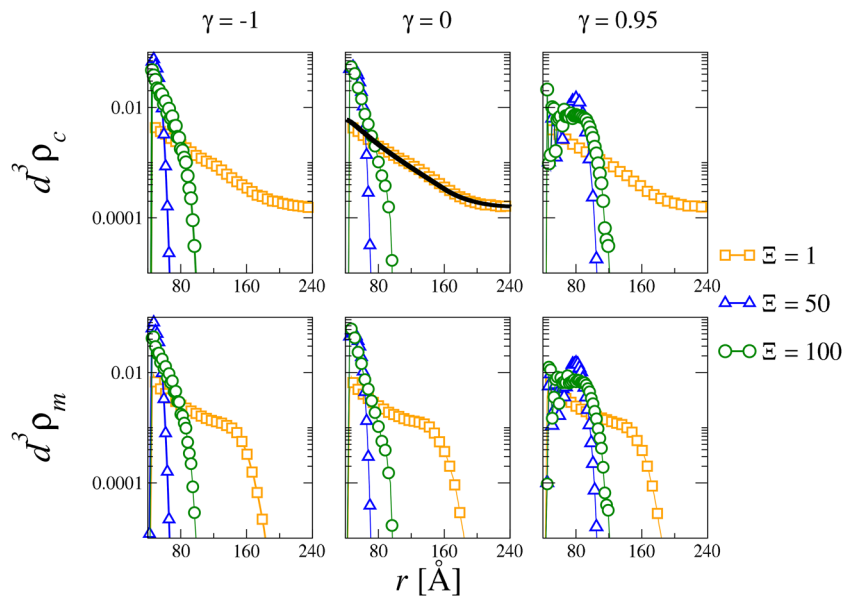
FIG. 2. Concentration profiles of counterions (top figures) and polyelectrolyte monomers (bottom figures). Charged chains have $N_m = 30$ monomers, while the nano-core radius is 40 Å. The metallic, unpolarizable, and dielectric cases are shown in the left, middle, and right columns, respectively. Three coupling parameters are considered: $\Xi = 1$, $\Xi = 50$, and $\Xi = 100$, which correspond to orange, blue, and green symbols. The black line is the adjusted solution of the mPB equation.
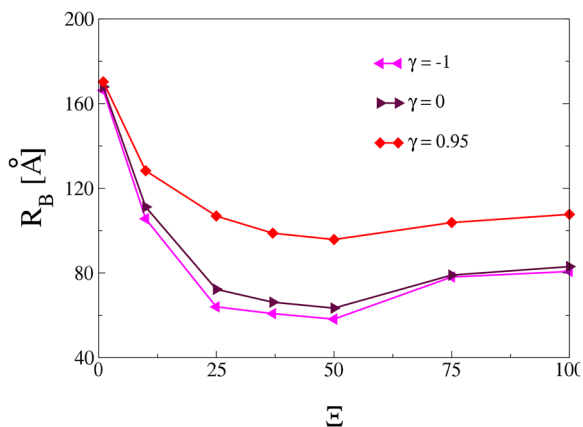

FIG. 3. PEB size, defined as the average distance between the nano-core center and the further monomer in each chain. The parameters are the same as those described in Fig. 2.
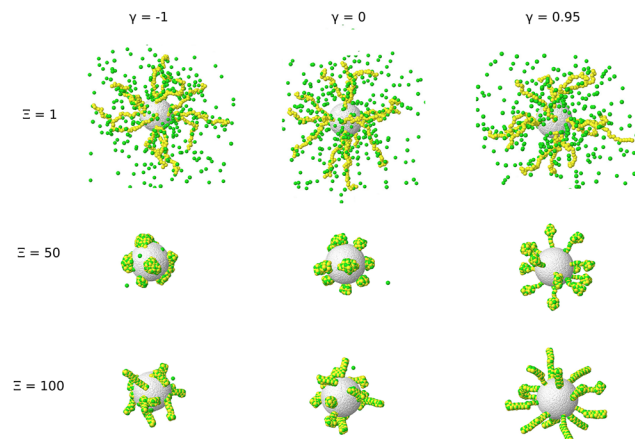

FIG. 4. Snapshots of equilibrated simulations. The parameters are the same as those described in Fig. 2. The yellow spheres represent the chain monomers, while the green spheres represent counterions. The white spheres (gray volume) represent the surface of the nanoparticle.

the regime of strong coupling are able to shrink the PEBs.[34] It is clear that the brush weakly re-swells for higher coupling parameters and a minimum can be seen in curves. The curves for unpolarizable and metallic cases are very similar, while much bigger PEBs are reported with a dielectric nano-core. The discussed effect can be visually observed[62] in the snapshots shown in Fig. 4. For the dielectric case, we also observe an interesting effect at the coupling $\Xi = 50$, the formation of tree-like structures, caused by the competition between ionic attraction to charged chains and ionic repulsion from the dielectric surface. For the coupling $\Xi = 100$, the effect is no

longer observed, showing that the ion–chain interactions dominate over the ion–surface interactions.

B. Big nano-core

The big nano-core PEB is studied in this subsection. The nano-core radius is $a = 200$ Å, while the confining spherical cell radius is $R = 600$ Å. The number of monomers per charged chain is set to $N_m = 60$, while the number of polyelectrolyte chains is the same as in Sec. IV A, $N_p = 14$. The grafting density is 0.0027 chains per nm²
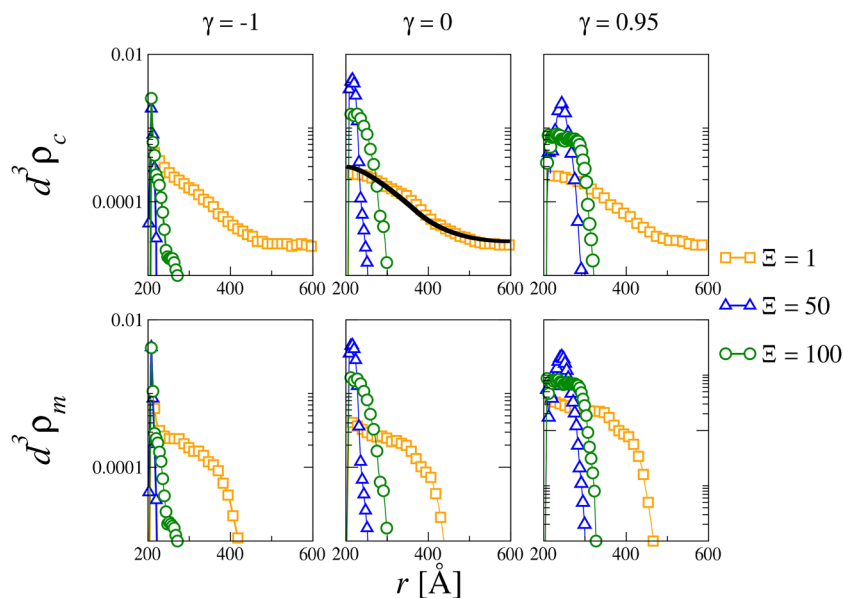
FIG. 5. Concentration profiles of counterions (top figures) and polyelectrolyte monomers (bottom figures). Charged chains have $N_m = 60$ monomers, while the nano-core radius is 200 Å. The metallic, unpolarizable, and dielectric cases are shown in the left, middle, and right columns, respectively. Three coupling parameters are considered: $\Xi = 1$, $\Xi = 50$, and $\Xi = 100$, which correspond to orange, blue, and green symbols, respectively. The black line is the solution of the mPB equation.
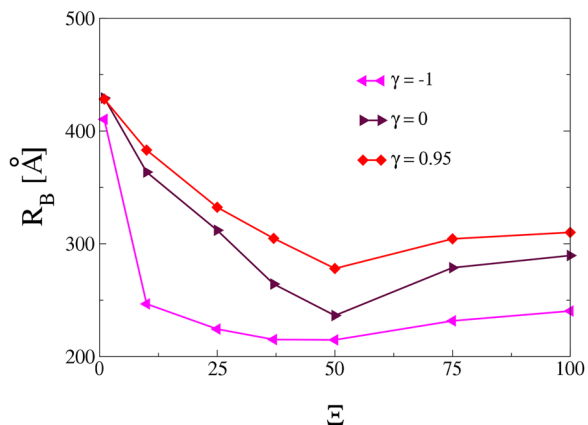
FIG. 6. PEB size, defined as the average distance between the nano-core center and the further monomer in each chain. The parameters are the same as those described in Fig. 5.

in this case. Such a low grafting density is considered when the interaction between solute and substrate is relevant.[63] Again, we study more deeply the cases with electrostatic coupling parameters $\Xi = 1$, 50, and 100, for metallic, $\gamma = -1$, unpolarizable, $\gamma = 0$, and dielectric nano-cores, $\gamma = 0.95$. The ionic and monomer concentration profiles are shown in Fig. 5. The mean-field theory is used for the weak coupling and unpolarizable case; see the black line in the mentioned figure. We use the same constant $b = 11$ in Eq. (7) and in the mPB equation, Eq. (5), fitted for the previous case.

It can be seen that, for higher coupling parameters, the ionic and monomeric adsorptions to PEBs are strong. Counterintuitively,

the ionic adsorption for parameter $\Xi = 100$ is weaker than for $\Xi = 50$, for all nano-core polarizations. The PEB is less condensed for the coupling $\Xi = 100$ than for $\Xi = 50$. Again, this is a property that is absent in charged colloids but seems to be present in PEBs. As in the previously studied small nano-core PEBs, a moderate shrinking–swelling effect is also observed for big nano-core PEBs; see Fig. 6.

Interestingly, for the present case, the charged chain condensation has a different nature for metallic nano-cores. Plenty of counterions attach directly to the metallic surface due to image charge interaction, leaving the charged chains with an excess of charge. This results in non-neutralized charged chains, which strongly adsorb to the metallic nano-core surface due to image charge interactions. This tells us that the effect of surface polarization depends on the grafting density, as previously shown for planar surfaces.[48,49] The effect can be seen in the snapshots of equilibrated simulations;[62] see Fig. 7. The snapshots for the metallic case with high coupling parameters show that some of the counterions adsorbed to the surface, instead of chains. The fractions of counterions adsorbed to the surface are around 30% and 17% for couplings $\Xi = 50$ and $\Xi = 100$, respectively, meaning that the average chain charge neutralization is around 70% and 83%, respectively. Some of these ions act as chain–surface linkers, ≈ 17 and 30% for couplings $\Xi = 50$ and $\Xi = 100$, respectively, qualitatively similar to what is found for planar surfaces.[49] For comparison, the fractions of adsorbed counterions to the small nano-core brush are less than 1%. This does not happen for unpolarizable and insulating nano-cores; see other snapshots in Fig. 7. As in the small nano-core case, the charged chains form a tree-like structure in the insulating nano-core, the counterions adsorb in a way to prefer to stay more condensed in the further region of charged chains. The cause of the effect is the electrostatic repulsion from image charges in the insulating material. As can be seen in the last drawing of Fig. 7, the
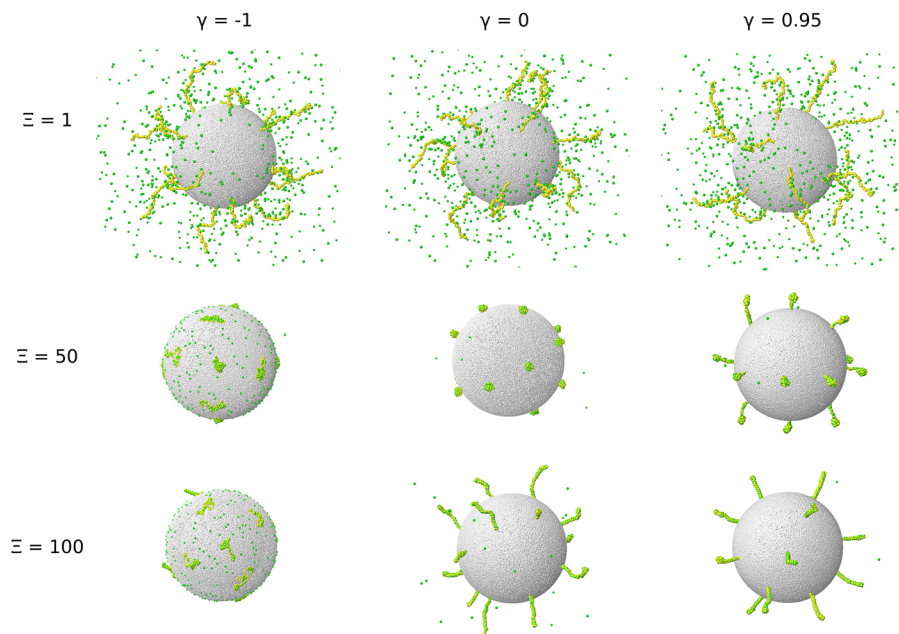
FIG. 7. Snapshots of equilibrated simulations. The parameters are the same as those described in Fig. 5. The yellow spheres represent the chain monomers, while the green spheres represent counterions. The white spheres (gray volume) represent the surface of the nanoparticle.

effect is almost entirely absent in the higher electrostatic coupling regime, $\Xi = 100$.

V. CONCLUSIONS

In this work, we study the roles of brush nano-core polarization and electrostatic coupling in the structure of spherical polyelectrolyte brushes and the distribution of counterions around them. We use the method of image charges to take into account surface polarization. The dynamics are performed with the Langevin method. A modified Poisson–Boltzmann theory is used to describe the ionic concentrations around the brush in the case of weak electrostatic coupling and unpolarizable nano-core. We show that the grafting density of chains is important for polarization effects. For small nano-core PEBs or higher grafting density, the results obtained with metallic or unpolarizable nano-cores are almost the same, while the results for dielectric nano-core show relevant differences. This can be explained by the fact that, in metallic and unpolarizable cases, there is always a counterion attraction toward the surface, with more chance to counterion-chain binding due to the high grafting density, differently from the dielectric case in which charge repulsion takes place. In the case of big nanoparticles, or lower grafting density, we show that the metallic nature of brush nano-core is much more efficient to shrink the polyelectrolyte brush in comparison with the unpolarizable or dielectric case. For moderate electrostatic couplings, the counterions attach directly to the brush nano-core, leaving the charged chains not neutralized. This allows them to adsorb to the nanoparticle surface, also by image charge interactions. For both small and big dielectric nano-cores, the effect is different: the counterions tend to neutralize the charged chains forming tree-like structures in the intermediate coupling regime due to image charge repulsion. For higher electrostatic couplings, the structures are more stretched, increasing the size of PEBs when a shrinking–swelling phenomenon takes place.

AUTHOR DECLARATIONS

Conflict of Interest

The authors have no conflicts to disclose.

Author Contributions

Igor M. Telles: Data curation (equal). **Muhammad Arfan**: Data curation (equal). **Alexandre P. dos Santos**: Conceptualization (equal).

DATA AVAILABILITY

The data that support the findings of this study are available within the article.

REFERENCES

[1] J. Rühe, M. Ballauff, M. Biesalski, P. Dziezok, F. Gröhn, D. Johannsmann, N. Houbenov, N. Hugenberg, R. Konradi, S. Minko, M. Motornov, R. R. Netz, M. Schmidt, C. Seidel, M. Stamm, T. Stephan, D. Usov, and H. Zhang, "Polyelectrolyte brushes," in *Polyelectrolytes with Defined Molecular Architecture I*, edited by M. Schmidt (Springer, Berlin, Heidelberg, 2004), pp. 79–150.

[2] S. Minko, J. Macromol. Sci. C **46**, 397 (2006).

22 May 2024 20:38:57

[3] M. Ballauff and O. Borisov, Curr. Opin. Colloid Interface Sci. **11**, 316 (2006).

[4] M. Ballauff, Prog. Polym. Sci. **32**, 1135 (2007).

[5] S. Das, M. Banik, G. Chen, S. Sinha, and R. Mukherjee, Soft Matter **11**, 8550 (2015).

[6] T. Kreer, Soft Matter **12**, 3479 (2016).

[7] Y. Higaki, M. Kobayashi, D. Murakami, and A. Takahara, Polym. J. **48**, 325 (2016).

[8] Z. He, W. J. Xie, Z. Liu, G. Liu, Z. Wang, Y. Q. Gao, and J. Wang, Sci. Adv. **2**, e1600345 (2016).

[9] M. Kobayashi, Y. Terayama, H. Yamaguchi, M. Terada, D. Murakami, K. Ishihara, and A. Takahara, Langmuir **28**, 7212 (2012).

[10] Z. Zeng, Y. Ai, and S. Qian, Phys. Chem. Chem. Phys. **16**, 2465 (2014).

[11] J.-Y. Lin, C.-Y. Lin, J.-P. Hsu, and S. Tseng, Anal. Chem. **88**, 1176 (2016).

[12] C.-Y. Lin, J.-P. Hsu, and L.-H. Yeh, Sens. Actuators, B **258**, 1223 (2018).

[13] Q. Cao, C. Zuo, L. Li, Y. Zhang, and G. Yan, J. Polym. Sci., Part B: Polym. Phys. **50**, 805 (2012).

[14] G. Chen and S. Das, J. Phys. Chem. B **121**, 3130 (2017).

[15] M. Schrinner, F. Polzer, Y. Mei, Y. Lu, B. Haupt, M. Ballauff, A. Göldel, M. Drechsler, J. Preussner, and U. Glatzel, Macromol. Chem. Phys. **208**, 1542 (2007).

[16] G. Sharma and M. Ballauff, Macromol. Rapid Commun. **25**, 547 (2004).

[17] Y. Yuan and B. Liu, ACS Appl. Mater. Interfaces **6**, 14903 (2014).

[18] M. Fuller and I. Köper, Polymers **10**, 1336 (2018).

[19] I. E. Dunlop, R. K. Thomas, S. Titmus, V. Osborne, S. Edmondson, W. T. S. Huck, and J. Klein, Langmuir **28**, 3187 (2012).

[20] R. Choueiri, E. Galati, H. Thérien-Aubin, A. Klinkova, E. Larin, A. Querejeta-Fernández, L. Han, H. Xin, O. Gang, E. Zhulina, M. Rubinstein, and E. Kumacheva, Nature **538**, 79 (2016).

[21] G. Aktas Eken and C. K. Ober, Macromolecules **55**, 5291 (2022).

[22] M. Karimzadeh, M. Khatibi, and S. N. Ashrafizadeh, Phys. Fluids **34**, 122008 (2022).

[23] P. González-Mozuelos and M. O. de la Cruz, J. Chem. Phys. **103**, 3145 (1995).

[24] M. Biesalski and J. Rühe, Langmuir **16**, 1943 (2000).

[25] T. Jiang, Z. Li, and J. Wu, Macromolecules **40**, 334 (2007).

[26] L. Chen, H. Merlitz, S.-z. He, C.-X. Wu, and J.-U. Sommer, Macromolecules **44**, 3109 (2011).

[27] X. Chu, J. Yang, G. Liu, and J. Zhao, Soft Matter **10**, 5568 (2014).

[28] C. J. Galvin, M. D. Dimitriou, S. K. Satija, and J. Genzer, J. Am. Chem. Soc. **136**, 12737 (2014).

[29] Y. Luo, C. Wang, A.-P. Pang, X. Zhang, D. Wang, and X. Lu, Macromolecules **54**, 6006 (2021).

[30] J. Zhang, R. Kou, and G. Liu, Langmuir **33**, 6838 (2017).

[31] H. Merlitz, C. Li, C. Wu, and J.-U. Sommer, Soft Matter **11**, 5688 (2015).

[32] Y. Rakita, D. Golodnitsky, and A. Natan, J. Electrochem. Soc. **161**, E3049 (2014).

[33] X. Guo and K. Zhao, J. Phys.: Condens. Matter **29**, 055102 (2016).

[34] J. Yu, J. Mao, G. Yuan, S. Satija, Z. Jiang, W. Chen, and M. Tirrell, Macromolecules **49**, 5609 (2016).

[35] A. Naji, R. R. Netz, and C. Seidel, Eur. Phys. J. E **12**, 223 (2003).

[36] K. Ehtiati, S. Z. Moghaddam, H.-A. Klok, A. E. Daugaard, and E. Thormann, Macromolecules **55**, 5123 (2022).

[37] H. Ouyang, Z. Xia, and J. Zhe, Microfluid. Nanofluid. **9**, 915 (2010).

[38] Q. Wei, M. Cai, F. Zhou, and W. Liu, Macromolecules **46**, 9368 (2013).

[39] Y. Mei and M. Ballauff, Eur. Phys. J. E **16**, 341 (2005).

[40] A. P. dos Santos and R. R. Netz, J. Chem. Phys. **148**, 164103 (2018).

[41] A. P. dos Santos, A. Bakhshandeh, and Y. Levin, J. Chem. Phys. **135**, 044124 (2011).

[42] A. Bakhshandeh, A. P. dos Santos, and Y. Levin, Phys. Rev. Lett. **107**, 107801 (2011).

[43] K. Barros and E. Luijten, Phys. Rev. Lett. **113**, 017801 (2014).

[44] T. D. Nguyen, F. Jiménez-Ángeles, and M. Olvera de la Cruz, J. Chem. Phys. **155**, 194901 (2021).

[45] I. M. Telles and A. P. dos Santos, Langmuir **37**, 2104 (2021).

[46] R. K. Bombardelli, I. M. Telles, A. P. dos Santos, and Y. Levin, J. Phys. Chem. B **125**, 11091 (2021).

[47] V. B. Tergolina and A. P. dos Santos, J. Chem. Phys. **147**, 114103 (2017).

[48] J. Yuan, H. S. Antila, and E. Luijten, ACS Macro Lett. **8**, 183 (2019).

[49] J. Yuan, H. S. Antila, and E. Luijten, Macromolecules **53**, 2983 (2020).

[50] D. Frenkel and B. Smith, *Understanding Molecular Simulation* (Academic Press, New York, 1996).

[51] M. G. Paterlini and D. M. Ferguson, Chem. Phys. **236**, 243 (1998).

[52] J. D. Jackson, *Classical Electrodynamics* (Wiley, New York, 1999).

[53] R. S. Dias, A. A. C. C. Pais, P. Linse, M. G. Miguel, and B. Lindman, J. Phys. Chem. B **109**, 11781 (2005).

[54] G. S. Manning, J. Chem. Phys. **51**, 924 (1969).

[55] B. Petersen, R. Roa, J. Dzubiella, and M. Kanduč, Soft Matter **14**, 4053 (2018).

[56] S. Misra, S. Varanasi, and P. P. Varanasi, Macromolecules **22**, 4173 (1989).

[57] F. von Goeler and M. Muthukumar, Macromolecules **28**, 6608 (1995).

[58] R. R. Netz and D. Andelman, Phys. Rep. **380**, 1 (2003).

[59] A. Bakhshandeh, M. Segala, and T. Escobar Colla, Macromolecules **55**, 35 (2022).

[60] O. J. Hehmeyer, G. Arya, A. Z. Panagiotopoulos, and I. Szleifer, J. Chem. Phys. **126**, 244902 (2007).

[61] Y. Levin, Rep. Prog. Phys. **65**, 1577 (2002).

[62] See http://www.jmol.org/ for Jmol: an open-source Java viewer for chemical structures in 3D.

[63] W. J. Brittain and S. Minko, J. Polym. Sci., Part A: Polym. Chem. **45**, 3505 (2007).

22 May 2024 20:38:57